1-1-2013

Study On Covolume-Upwind Finite Volume Approximations For Linear Parabolic Partial Differential Equations

Rosalia Tatano
University of South Carolina

Study on Covolume-Upwind Finite Volume Approximations for Linear Parabolic Partial Differential Equations

by

Rosalia Tatano

Bachelor of Science
University of Palermo, 2010

Submitted in Partial Fulfillment of the Requirements

For the Degree of Master of Science in

Mathematics

College of Arts and Sciences

University of South Carolina

2013

Accepted by:

Lili Ju, Major Professor

Xinfeng Liu, Reader

Lacy Ford, Vice Provost and Dean of Graduate Studies

Dedication

To my husband Antonio, who supported me with his love throughout the course of my studies and to my little child Samuele.

Acknowledgments

I am greatly indebted to my advisor Dr. Lili Ju for his precious help and guidance through this work of thesis. With his enthusiasm, his inspiration, and his great efforts to explain things clearly and simply, he helped to make my research fun for me. Throughout my period at the University of South Carolina, he provided encouragement, warm support and good teaching. I would have been lost without him.

I would like to sincerely thank my committee member Prof. Xinfeng Liu for his time and accessibility.

I would like to express my sincere gratitude to Prof. Ognian Trifonov and Ms. Heather Covey for helping and assisting me in many different ways during the entire period of my study and especially when I first arrived at USC.

I would like to thank also my colleagues at USC for providing a stimulating and fun environment in which to learn and grow. In particular, I am grateful to Heather Smith, Bethany Wentzky, Jennifer Tabat and Richard Oh for their friendship, help and useful advice.

Abstract

In this thesis we solve two-dimensional linear parabolic partial differential equations with pure Dirichelet boundary conditions, using the bilinear covolume-upwind finite volume method on rectangular grids to discretize the spatial variables and the Crank-Nicholson method for the time variable. These PDEs provide a model for problems from various fields of engineering and applied sciences, such as unsteady viscous flow problems, the simulation of oil extraction from underground reservoirs, transport of air and ground water pollutants and modeling of semiconductor devices. Finite volume method has the important advantage of allowing the conversion of integrations over the control volume to integrations over its boundary based on Green's Theorem. Then, one can use quadrature rules to approximate the resulting integrals. In order to avoid non-physical oscillations that can arise from the numerical solution of convection-dominated problems when using the central finite volume scheme, we generate non-standard control volumes using local Peclet's numbers and the upwind principle. We numerically compare the covolume-upwind finite volume method with the central and the upwind finite volume schemes, demonstrating stability and better convergence of the method through various examples.

Table of Contents

List of Tables

List of Figures

Chapter 1

Introduction

1.1 Literature review

Linear parabolic partial differential equations arise in many applications of science and engineering, such as transport of ground water pollutants, oil reservoir flow, semiconductor devices modeling, meteorology. Finite difference methods (FDMs) were first implemented to solve these problems, together with finite element methods (FEMs) [5]. In the finite element method, the derivatives are replaced by difference quotients which involve only function values at the grid points. The method is simply to implement, but it is not good when the equation has discontinuous coefficients or one has to handle complex geometry in multiple dimensions. FEMs are based on the variational formulation of the problem. Then the variational formulation is discretized in a finite dimensional space. For a more detailed description of these methods refer to [3] and [6].

The basic idea of finite volume methods (FVMs) is to discretize the domain in subdomains, called control volumes or covolumes, which form a partition of the original domain. Then, one integrates the whole equation over each covolume and applies the divergence theorem to transform these integrals to integrals over the boundary of the covolumes. FEMs and FVMs share some good properties: flexibility with respect to the geometry of the domain, simple discretization of the boundary conditions, possibility of using unstructured grids. FVMs were extensively used in many engineering fields, such as fluid mechanics and heat transfer. Finite volume methods

for convection-diffusion problem were introduced in the sixties by Samarkii [20] and developed by Patankar [18] in the eighties. A posteriori error estimates for the non-stationary convection-diffusion-reaction problem were found by Verfurth in [26] and by Nochetto, Akrivis and Makridakis in [2]. A modification of finite volume schemes that is second-order accurate in time and fourth-order in space for the one-dimensional problem was presented in [15]. New schemes for solving the convection-diffusion equation, including adaptive schemes, are introduced in [1], [19], [25], [23], [24].

In several cases, the diffusive term of the convection-diffusion-reaction equation is smaller that the convective one. This kind of problems are called convection-dominated problems. When using classical methods to find the numerical solution of convection-dominated equations, non-physical oscillations may arise. To overcome this problem, several numerical methods have been introduced. For example, in [10], the author derived an upwind type method on triangular meshes. In [7], the authors studied stabilized FEMs for time-dependent convection-dominated problems, such as streamline-upwind Petrov-Galerkin method. To stabilize FEMs, adaptive mesh grids methods have also been introduced for example in [22]. Finally, in [8], a Crank-Nicholson finite difference scheme with a midpoint upwind finite difference operator on uniform mesh was derived. The authors proved that this method is second-order accurate in time and almost second-order accurate in space in a coarse mesh.

In this thesis, we extend the application of the bilinear covolume-upwind finite volume method (bilinear CUFVM) on rectangular grids introduced in [27] to the linear parabolic partial differential equations with homogeneous Dirichelet boundary conditions. This method uses local Peclet's numbers and the upwind idea to construct nonstandard control volumes and midpoint quadrature to get the discretized systems. This space disctretization, however, gives us only a semi-discretized system. Then, in order to get a fully discretization of the problem and thus, a numerical solution, we will use the Crank-Nicholson scheme to discretize the time variable. It will

be shown through numerical examples, that this method is second-order accurate in the L^2 norm and first-order in the H^1 norm and stable even for strongly convection-dominated problems. We will also compare this method to the central and the upwind finite volume methods.

This thesis is organized as follows: in the next section of this chapter we will describe the model problem and its variational formulation. In Chapter 2, we will derive the central and upwind finite volume methods, while the covolume-upwind finite volume method will be studied in Chapter 3. Convergence and stability of these methods will be proved through numerical examples in two dimensions in Chapter 4, followed by conclusions in Chapter 5.

1.2 The model problem

Let Ω be a bounded domain of $\mathbb{R}^d$ with piecewise polygonal boundary $\partial\Omega$ and set $\Omega_T = \Omega \times (0, T]$, for some fixed time $T > 0$. Let consider the parabolic differential equation

$$\begin{cases} u_t - \nabla \cdot (a\nabla u - \overrightarrow{\mathbf{b}}\, u) + ru = f, & \mathbf{x} \in \Omega,\ t \in (0, T] \\ u = 0, & \mathbf{x} \in \partial\Omega,\ t \in (0, T] \\ u = u_0(\mathbf{x}), & \mathbf{x} \in \Omega,\ t = 0 \end{cases} \tag{1.1}$$

where $a(\mathbf{x}, t) > a_0 > 0 \in \mathrm{H}^1(\Omega_T)$ is the diffusion rate, $\overrightarrow{\mathbf{b}}(\mathbf{x}, t) \in \mathrm{H}^1(\Omega_T)$ is the transport velocity, $r(\mathbf{x}, t) \geq 0 \in \mathrm{L}^\infty(\Omega_T)$ is the given reaction rate function, $u_0 \in \mathrm{L}^2(\Omega)$ is the given initial condition function and $f(\mathbf{x}, t) \in \mathrm{L}^2(\Omega_T)$ is a given source function. We assume also that

$$\frac{\nabla \cdot \overrightarrow{\mathbf{b}}}{2} + r \geq 0 \tag{1.2}$$

We want to write the variational formulation for the initial-boundary value problem (1.1). Let $v \in \mathrm{H}_0^1(\Omega)$. Then, multiplying the differential equation by v and integrating

over Ω, we get

$$\int_\Omega u_t v d\mathbf{x} - \int_\Omega \nabla \cdot (a\nabla u - \overrightarrow{\mathbf{b}} u) v d\mathbf{x} + \int_\Omega ruv d\mathbf{x} = \int_\Omega fv d\mathbf{x}$$

Using integration by parts and recalling that v vanishes on the boundary of Ω, the previous become

$$\int_\Omega u_t v d\mathbf{x} + \int_\Omega \left(a\nabla u - \overrightarrow{\mathbf{b}} u\right) \cdot \nabla v d\mathbf{x} + \int_\Omega ruv d\mathbf{x} = \int_\Omega fv d\mathbf{x}$$

Let us define

$$A(u,v) = \int_\Omega \left(a\nabla u \cdot \nabla v - (\overrightarrow{\mathbf{b}} u) \cdot \nabla v + ruv\right) d\mathbf{x}$$

for $u, v \in \mathrm{H}_0^1(\Omega)$.Then the weak formulation of the problem (1.1) is: Find $u = u(\cdot, t) \in \mathrm{H}_0^1(\Omega)$ $(0 \leq t \leq T)$ such that

$$\begin{cases} (u_t, v) + A(u,v) = (f,v), & \forall v \in \mathrm{H}_0^1(\Omega),\ t > 0 \\ u(\mathbf{x}, 0) = u_0(\mathbf{x}) & \mathbf{x} \in \Omega \end{cases} \tag{1.3}$$

where $(\cdot, \cdot)$ denotes the inner product of $\mathrm{L}_2(\Omega)$. The bilinear form $A(u,v)$ satisfies the following property

$$A(u,v) \leq c_1 \parallel u \parallel_1 \parallel v \parallel_1 \qquad \forall u, v \in \mathrm{H}_0^1(\Omega)$$

Moreover, there exists a constant $c_2 > 0$ such that

$$A(u,u) = \int_\Omega \left(a(\nabla u)^2 - (\overrightarrow{\mathbf{b}} u) \cdot \nabla u + ru^2\right) d\mathbf{x} \geq c_2 \parallel u \parallel_1^2 \qquad \forall u \in \mathrm{H}_0^1(\Omega)$$

This follows immediately from the assumptions on a, b, from (1.2) and the fact that (see [11])

$$\int_\Omega (\overrightarrow{\mathbf{b}} u) \cdot \nabla u d\mathbf{x} = -\frac{1}{2} \int_\Omega (\nabla \cdot \overrightarrow{\mathbf{b}}) u^2 d\mathbf{x}$$

Then, there exists a unique solution to the variational problem (1.3) [4].

Chapter 2

Standard finite volume methods

2.1 The control volume

Let consider the two-dimensional case of problem (1.1). In order to derive the central and the upwind finite volume methods for the given problem, we first need to construct the control volume. The notation used in the present work follows that one used in [27].

Let $\Omega = [x_l, x_r] \times [y_l, y_r]$. Let us define the partition of Ω as

$$x_l = x_0 < x_1 < \cdots < x_i < \cdots < x_{N_x} = x_r,$$

$$y_l = y_0 < y_1 < \cdots < y_j < \cdots < y_{N_y} = y_r,$$

where the grids are uniform and N_x and N_y are the numbers of grid blocks in the x and y directions respectively. Let $P_{i,j}$ denote the grid point of coordinates (x_i, y_j) and $\Delta x_i = x_i - x_{i-1}$, for $i = 1, \ldots, N_x$ and $\Delta y_j = y_j - y_{j-1}$, for $j = 1, \ldots, N_y$. We define the primary grid Ω_h for the finite volume approximation as

$$\{\Omega_{i,j} : \Omega_{i,j} = [x_{i-1}, x_i] \times [y_{j-1}, y_j],\ i = 1, \ldots, N_x,\ j = 1, \ldots, N_y\}$$

We want to construct the dual partition Ω_h^* of Ω with respect to the rectangulation Ω_h. If $P_{i,j}$ is an interior grid point, we construct its control volume $\Omega_{i,j}^*$ by connecting the centers of all its four adjacent cells, as in Figure 2.1. Then the set of the control volumes or covolumes is

$$\Omega_h^* = \{\Omega_{i,j}^* : i = 1, \ldots, N_x - 1,\ j = 1, \ldots, N_y - 1\}$$

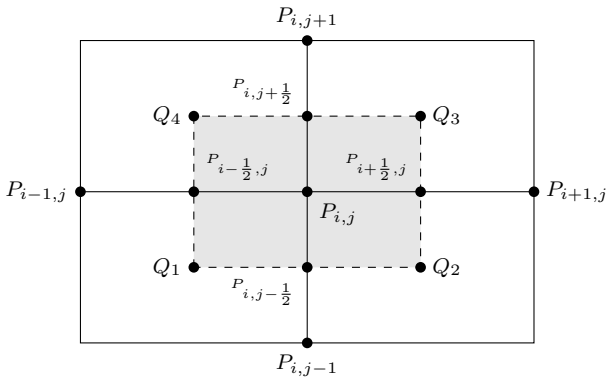

Figure 2.1 Control volume associated with the interior grid point $P_{i,j}$ for uniform grid.

Let us define

$$\mathbf{P}_\Omega = \{P_{i,j} : i = 0, \ldots, N_x,\ j = 0, \ldots, N_y\}, \tag{2.1}$$

$$\mathbf{P} = \{P_{i,j} : P_{i,j} \notin \partial\Omega,\ i = 0, \ldots, N_x,\ j = 0, \ldots, N_y\} \tag{2.2}$$

$$\mathbf{P}_D = \mathbf{P}_\Omega \backslash \mathbf{P} \tag{2.3}$$

Let us set the trial function space U_h to be the space of piecewise bilinear functions on the rectangular grid Ω_h

$$U_h = \{u_h \in C(\bar{\Omega}) : u_h|_{\Omega_{i,j}} \text{ is a bilinear function for any } \Omega_{i,j} \in \Omega_h\} \tag{2.4}$$

and the test function space V_h to be the space of piecewise constant function space over the dual partition Ω_h^*

$$V_h = \{v_h \in \mathrm{L}_2(\bar{\Omega}) : v_h|_{\Omega^*_{i,j}} = \text{constant for any } \Omega^*_{i,j} \in \Omega^*_h \text{ and } v_h|_{\Omega^*_{i,j}} = 0 \text{ if } P_{i,j} \in \mathbf{P}_D\}$$

Let $\{\phi_{i,j},\ (i,j) \in \mathbf{P}_\Omega\}$ be a basis of U_h such that $\phi_{i,j}$ is equal to 1 at $P_{i,j}$ and 0 otherwise and let $\{\psi_{i,j},\ (i,j) \in \mathbf{P}\}$ be a basis of V_h, where $\psi_{i,j}$ are the characteristic

functions of the covolume $\Omega^*_{i,j}$ defined as

$$\psi_{i,j}(\mathbf{x}) = \begin{cases} 1, & \mathbf{x} \in \Omega^*_{i,j} \\ 0, & \mathbf{x} \in \Omega / \Omega^*_{i,j} \end{cases}$$

Then $u_h \in U_h$ can be written as

$$u_h = \sum_{P_{i,j} \in \mathbf{P}_\Omega} u_{i,j} \phi_{i,j}$$

where $u_{i,j} = u_h(P_{i,j})$.

Multiplying the differential equation of (1.1) by $v_h \in V_h$, integrating over Ω and applying Green's formula on each $\Omega^*_{i,j}$, and replacing u with $u_h \in U_h$, we get the discrete approximation for the problem (1.1): Find $u_h = u_h(\cdot, t) \in U_h$ $(0 \le t \le T)$ such that

$$\begin{cases} B_h(\partial_t u_h, v_h) + A_h(u_h, v_h) = L_h(f, v_h) \quad \forall v_h \in V_h,\ t_n > 0 \\ u_h(\mathbf{x}, 0)|_{\mathbf{P}_D} = u_0(\mathbf{x}) \end{cases} \tag{2.5}$$

where

$$B_h(\partial_t u_h, v_h) = \sum_{P_{i,j} \in \mathbf{P}} v_h(P_{i,j}) \int_{\Omega^*_{i,j}} \partial_t u_h d\mathbf{x}, \tag{2.6}$$

$$\begin{aligned} A_h(u_h, v_h) = & - \sum_{P_{i,j} \in \mathbf{P}} v_h(P_{i,j}) \int_{\partial\Omega^*_{i,j}} (a \nabla u_h) \cdot \overrightarrow{\nu}_{i,j} ds \\ & + \sum_{P_{i,j} \in \mathbf{P}} v_h(P_{i,j}) \int_{\partial\Omega^*_{i,j}} (\overrightarrow{\mathbf{b}} \cdot \overrightarrow{\nu}_{i,j}) u_h ds \\ & + \sum_{P_{i,j} \in \mathbf{P}} v_h(P_{i,j}) \int_{\Omega^*_{i,j}} r u_h d\mathbf{x} \end{aligned} \tag{2.7}$$

and

$$L_h(f, v_h) = \sum_{P_{i,j} \in \mathbf{P}} v_h(P_{i,j}) \int_{\Omega^*_{i,j}} f d\mathbf{x} \tag{2.8}$$

where $\nu_{i,j}$ is the unit outward normal along $\Omega^*_{i,j}$.

Till now we have got a semi-discrete scheme by discretizing the space variable. In order to get a numerical solution of problem (1.1), we need to discretize also the time

variable, to obtain a fully-discrete scheme.

Let us denote with $\Delta t = T/N_t$ the time step size and let $t_n = n\Delta t$ ($n = 0, \ldots, N_t + 1$). At each time $t = t_n$, using the difference quotient

$$\bar{\partial}_t u_h^n = \frac{u_h^{n+1} - u_h^n}{\Delta t} \tag{2.9}$$

to approximate $\partial_t u_h$ and using Crank-Nicolson scheme, we get that the variational problem becomes: Find $u_h^n \in U_h$ such that

$$\begin{cases} B_h(\bar{\partial}_t u_h^n, v_h) + A_h\left(\frac{u_h^{n+1}+u_h^n}{2}, v_h\right) = L_h\left(\frac{f^{n+1}+f^n}{2}, v_h\right) \quad \forall v_h \in V_h,\ n = 1, 2, \ldots \\ u_h^0|_{\mathbf{P}} = u_0 \end{cases} \tag{2.10}$$

For a given u_h^n, we have

$$A_h(u_h^{n+1}, v_h) + \frac{1}{\Delta t}(u_h^{n+1}, v_h) \geq c \parallel u_h^{n+1} \parallel_1^2 \qquad \forall u_h^{n+1} \in U_h$$

This guarantees the existence and uniqueness of the solution u_h^{n+1} to (2.10) for a given u_h^n [12].

Setting $v_h = \psi_{i,j}$ in the expressions (2.6)-(2.8) and using the proposed time discretization, we get

$$\begin{aligned} \int_{\Omega_{i,j}^*} \frac{u_h^{n+1} - u_h^n}{\Delta t} d\mathbf{x} \quad &- \quad \int_{\partial\Omega_{i,j}^*} \frac{(a^{n+1}\nabla u_h^{n+1}) \cdot \overrightarrow{\nu}_{i,j} + (a^n \nabla u_h^n) \cdot \overrightarrow{\nu}_{i,j}}{2} ds \\ &+ \quad \int_{\partial\Omega_{i,j}^*} \frac{(\overrightarrow{\mathbf{b}}^{n+1} \cdot \overrightarrow{\nu}_{i,j}) u_h^{n+1} + (\overrightarrow{\mathbf{b}}^n \cdot \overrightarrow{\nu}_{i,j}) u_h^n}{2} ds \\ &+ \quad \int_{\Omega_{i,j}^*} \frac{r^{n+1} u_h^{n+1} + r^n u_h^n}{2} d\mathbf{x} = \int_{\Omega_{i,j}^*} \frac{f^{n+1} + f^n}{2} d\mathbf{x} \end{aligned} \tag{2.11}$$

Rearranging the terms, we get

$$\begin{aligned} \int_{\Omega_{i,j}^*} u_h^{n+1} d\mathbf{x} \quad &- \quad \frac{\Delta t}{2} \int_{\partial\Omega_{i,j}^*} (a^{n+1}\nabla u_h^{n+1}) \cdot \overrightarrow{\nu}_{i,j} ds \\ &+ \quad \frac{\Delta t}{2} \int_{\partial\Omega_{i,j}^*} (\overrightarrow{\mathbf{b}}^{n+1} \cdot \overrightarrow{\nu}_{i,j}) u_h^{n+1} ds + \frac{\Delta t}{2} \int_{\Omega_{i,j}^*} r^{n+1} u_h^{n+1} d\mathbf{x} \\ &= \quad \int_{\Omega_{i,j}^*} u_h^n d\mathbf{x} + \frac{\Delta t}{2} \int_{\partial\Omega_{i,j}^*} (a^n \nabla u_h^n) \cdot \overrightarrow{\nu}_{i,j} ds - \frac{\Delta t}{2} \int_{\partial\Omega_{i,j}^*} (\overrightarrow{\mathbf{b}}^n \cdot \overrightarrow{\nu}_{i,j}) u_h^n ds \\ &- \quad \frac{\Delta t}{2} \int_{\Omega_{i,j}^*} r^n u_h^n d\mathbf{x} + \frac{\Delta t}{2} \int_{\Omega_{i,j}^*} (f^{n+1} + f^n) d\mathbf{x} \end{aligned} \tag{2.12}$$

2.2 The central scheme

To get the central finite volume scheme (CFVM), we approximate each term of the equation (2.12) using the second-order accurate midpoint rule. We will consider each term separately. Let $P_{i,j} \in \mathbf{P}$ be an interior point (Figure 2.1). For the first member, we have

$$\int_{\Omega^*_{i,j}} u_h^{n+1} d\mathbf{x} \approx u_h^{n+1}(P_{i,j})\ Area(Q_1Q_2Q_3Q_4) \tag{2.13}$$

$$\begin{aligned}
-\int_{\partial\Omega^*_{i,j}} (a^{n+1}\nabla u_h^{n+1})\cdot\overrightarrow{\nu}_{i,j} ds \approx & + \frac{\partial u_h^{n+1}}{\partial y}\left(P_{i,j-\frac{1}{2}}\right)\int_{\overline{Q_1Q_2}} a^{n+1} ds - \frac{\partial u_h^{n+1}}{\partial x}\left(P_{i+\frac{1}{2},j}\right)\int_{\overline{Q_2Q_3}} a^{n+1} ds \\
& - \frac{\partial u_h^{n+1}}{\partial y}\left(P_{i,j+\frac{1}{2}}\right)\int_{\overline{Q_3Q_4}} a^{n+1} ds + \frac{\partial u_h^{n+1}}{\partial x}\left(P_{i-\frac{1}{2},j}\right)\int_{\overline{Q_4Q_1}} a^{n+1} ds \\
= & + \frac{u_{i,j}^{n+1} - u_{i,j-1}^{n+1}}{\Delta y_j}\int_{\overline{Q_1Q_2}} a^{n+1} ds - \frac{u_{i+1,j}^{n+1} - u_{i,j}^{n+1}}{\Delta x_{i+1}}\int_{\overline{Q_2Q_3}} a^{n+1} ds \\
& - \frac{u_{i,j+1}^{n+1} - u_{i,j}^{n+1}}{\Delta y_{j+1}}\int_{\overline{Q_3Q_4}} a^{n+1} ds + \frac{u_{i,j}^{n+1} - u_{i-1,j}^{n+1}}{\Delta x_i}\int_{\overline{Q_4Q_1}} a^{n+1} ds
\end{aligned} \tag{2.14}$$

$$\begin{aligned}
\int_{\partial\Omega^*_{i,j}} (\overrightarrow{\mathbf{b}}^{n+1}\cdot\overrightarrow{\nu}_{i,j}) u_h^{n+1} ds \approx & - u_{i,j-\frac{1}{2}}^{n+1}\int_{\overline{Q_1Q_2}} b_y^{n+1} ds + u_{i+\frac{1}{2},j}^{n+1}\int_{\overline{Q_2Q_3}} b_x^{n+1} ds \\
& + u_{i,j+\frac{1}{2}}^{n+1}\int_{\overline{Q_3Q_4}} b_y^{n+1} ds - u_{i-\frac{1}{2},j}^{n+1}\int_{\overline{Q_4Q_1}} b_x^{n+1} ds \\
= & - \frac{u_{i,j-1}^{n+1} + u_{i,j}^{n+1}}{2}\int_{\overline{Q_1Q_2}} b_y^{n+1} ds + \frac{u_{i,j}^{n+1} + u_{i+1,j}^{n+1}}{2}\int_{\overline{Q_2Q_3}} b_x^{n+1} ds \\
& + \frac{u_{i,j}^{n+1} + u_{i,j+1}^{n+1}}{2}\int_{\overline{Q_3Q_4}} b_y^{n+1} ds - \frac{u_{i-1,j}^{n+1} + u_{i,j}^{n+1}}{2}\int_{\overline{Q_4Q_1}} b_x^{n+1} ds
\end{aligned} \tag{2.15}$$

$$\int_{\Omega^*_{i,j}} r^{n+1} u_h^{n+1} d\mathbf{x} \approx u_h^{n+1}(P_{i,j})\int_{Q_1Q_2Q_3Q_4} r^{n+1} d\mathbf{x} \tag{2.16}$$

Similarly, the right hand side becomes

$$\int_{\Omega^*_{i,j}} u_h^{n} d\mathbf{x} \approx u_h^{n}(P_{i,j})\ Area(Q_1Q_2Q_3Q_4) \tag{2.17}$$

$$\begin{aligned}
\int_{\partial\Omega^*_{i,j}} (a^{n}\nabla u_h^{n})\cdot\overrightarrow{\nu}_{i,j} ds \approx & - \frac{\partial u_h^{n}}{\partial y}\left(P_{i,j-\frac{1}{2}}\right)\int_{\overline{Q_1Q_2}} a^{n} ds + \frac{\partial u_h^{n}}{\partial x}\left(P_{i+\frac{1}{2},j}\right)\int_{\overline{Q_2Q_3}} a^{n} ds \\
& + \frac{\partial u_h^{n}}{\partial y}\left(P_{i,j+\frac{1}{2}}\right)\int_{\overline{Q_3Q_4}} a^{n} ds - \frac{\partial u_h^{n}}{\partial x}\left(P_{i-\frac{1}{2},j}\right)\int_{\overline{Q_4Q_1}} a^{n} ds \\
= & - \frac{u_{i,j}^{n} - u_{i,j-1}^{n}}{\Delta y_j}\int_{\overline{Q_1Q_2}} a^{n} ds + \frac{u_{i+1,j}^{n} - u_{i,j}^{n}}{\Delta x_{i+1}}\int_{\overline{Q_2Q_3}} a^{n} ds \\
& + \frac{u_{i,j+1}^{n} - u_{i,j}^{n}}{\Delta y_{j+1}}\int_{\overline{Q_3Q_4}} a^{n} ds - \frac{u_{i,j}^{n} - u_{i-1,j}^{n}}{\Delta x_i}\int_{\overline{Q_4Q_1}} a^{n} ds
\end{aligned} \tag{2.18}$$

$$
\begin{aligned}
-\int_{\partial\Omega^*_{i,j}} (\overrightarrow{\mathbf{b}}^n \cdot \overrightarrow{\nu}_{i,j}) u_h^n ds \approx & + u^n_{i,j-\frac{1}{2}} \int_{\overline{Q_1Q_2}} b_y^n ds - u^n_{i+\frac{1}{2},j} \int_{\overline{Q_2Q_3}} b_x^n ds \\
& - u^n_{i,j+\frac{1}{2}} \int_{\overline{Q_3Q_4}} b_y^n ds + u^n_{i-\frac{1}{2},j} \int_{\overline{Q_4Q_1}} b_x^n ds \\
= & + \frac{u^n_{i,j-1}+u^n_{i,j}}{2} \int_{\overline{Q_1Q_2}} b_y^n ds - \frac{u^n_{i,j}+u^n_{i+1,j}}{2} \int_{\overline{Q_2Q_3}} b_x^n ds \\
& - \frac{u^n_{i,j}+u^n_{i,j+1}}{2} \int_{\overline{Q_3Q_4}} b_y^n ds + \frac{u^n_{i-1,j}+u^n_{i,j}}{2} \int_{\overline{Q_4Q_1}} b_x^n ds \qquad (2.19)
\end{aligned}
$$

$$
-\int_{\Omega^*_{i,j}} r^n u_h^n d\mathbf{x} \approx -u_h^n(P_{i,j}) \int_{Q_1Q_2Q_3Q_4} r^n d\mathbf{x} \qquad (2.20)
$$

This gives us a discrete system in $u(P_{i,j})$ for $P_{i,j} \in \mathbf{P}$ at the time $t = t_{n+1}$.

The central scheme is second-order convergent and it is stable only for sufficiently small mesh sizes. Moreover, non-physical numerical oscillations can arise using the central scheme when solving convection-dominated problems.

2.3 The upwind scheme

In the upwind scheme (UFVM), we use the same control volumes and time discretization defined in Section 2.1. The diffusion terms, the reaction terms and the first terms of each member of (2.12) will be discretized in the same way as in the central scheme. To obtain the discretization of the convection terms, let first define the following quantities:

$$
\begin{aligned}
B^{n+1}_{Q_1Q_2} &= \frac{1}{2}\left(\int_{Q_1Q_2} b_y^{n+1} ds + \left|\int_{Q_1Q_2} b_y^{n+1} ds\right|\right) \\
B^{n+1}_{Q_2Q_3} &= \frac{1}{2}\left(\int_{Q_2Q_3} b_x^{n+1} ds + \left|\int_{Q_2Q_3} b_x^{n+1} ds\right|\right) \\
B^{n+1}_{Q_3Q_4} &= \frac{1}{2}\left(\int_{Q_3Q_4} b_y^{n+1} ds + \left|\int_{Q_3Q_4} b_y^{n+1} ds\right|\right) \\
B^{n+1}_{Q_4Q_1} &= \frac{1}{2}\left(\int_{Q_4Q_1} b_x^{n+1} ds + \left|\int_{Q_4Q_1} b_x^{n+1} ds\right|\right)
\end{aligned}
$$

$$
\begin{aligned}
B^n_{Q_1Q_2} &= \frac{1}{2}\left(\int_{Q_1Q_2} b^n_y ds + \left|\int_{Q_1Q_2} b^n_y ds\right|\right)\\
B^n_{Q_2Q_3} &= \frac{1}{2}\left(\int_{Q_2Q_3} b^n_x ds + \left|\int_{Q_2Q_3} b^n_x ds\right|\right)\\
B^n_{Q_3Q_4} &= \frac{1}{2}\left(\int_{Q_3Q_4} b^n_y ds + \left|\int_{Q_3Q_4} b^n_y ds\right|\right)\\
B^n_{Q_4Q_1} &= \frac{1}{2}\left(\int_{Q_4Q_1} b^n_x ds + \left|\int_{Q_4Q_1} b^n_x ds\right|\right)
\end{aligned}
$$

Then we have

$$
\begin{aligned}
\int_{\partial\Omega_{i,j}{}^*} (\overrightarrow{\mathbf{b}}^{n+1} \cdot \overrightarrow{\nu}^{n+1}_{i,j}) u^{n+1}_h ds \approx \; & - \; B^{n+1}_{Q_1Q_2}(u^{n+1}_h(Q_1) + u^{n+1}_h(Q_2))\\
& + \; B^{n+1}_{Q_2Q_3}(u^{n+1}_h(Q_2) + u^{n+1}_h(Q_3))\\
& + \; B^{n+1}_{Q_3Q_4}(u^{n+1}_h(Q_3) + u^{n+1}_h(Q_4))\\
& - \; B^{n+1}_{Q_4Q_1}(u^{n+1}_h(Q_4) + u^{n+1}_h(Q_1)) \qquad (2.21)
\end{aligned}
$$

and

$$
\begin{aligned}
-\int_{\partial\Omega_{i,j}{}^*} (\overrightarrow{\mathbf{b}}^{n} \cdot \overrightarrow{\nu}^{n+1}_{i,j}) u^{n}_h ds \approx \; & + \; B^{n}_{Q_1Q_2}(u^{n}_h(Q_1) + u^{n}_h(Q_2))\\
& - \; B^{n}_{Q_2Q_3}(u^{n}_h(Q_2) + u^{n}_h(Q_3))\\
& - \; B^{n}_{Q_3Q_4}(u^{n}_h(Q_3) + u^{n}_h(Q_4))\\
& + \; B^{n}_{Q_4Q_1}(u^{n}_h(Q_4) + u^{n}_h(Q_1)) \qquad (2.22)
\end{aligned}
$$

As in the case of the central scheme, we obtain a discrete system in $u(P_{i,j})$ for $P_{i,j} \in \mathbf{P}$ at the time $t = t_{n+1}$. The upwind scheme is unconditionally stable, but it is only first-order convergent. However, high order accurate upwind schemes for convection-dominated problems have been proposed in [13]. A derivation of highly order accurate generalized upwind schemes on triangular mesh can be found in [12].

Chapter 3

Bilinear covolume-upwind finite volume method

3.1 The upwind-control volume

In the upwind scheme, for the discretization we take into account the grid points from the upwind sides, while in the central scheme we use the average of the point values from both sides. In a previous work [27], the bilinear covolume-upwind finite volume method for solving linear elliptic partial differential equations was introduced. In this method, the upwind idea was applied for the construction of a non-standard control volume for each grid point. We want extend the application of this method to the linear parabolic partial differential equation (1.1). Let us assume that the spatial and time discretizations defined in Section 2.1 hold. Let $\overrightarrow{\mathbf{b}}(\mathbf{x}) = (b_x(\mathbf{x}), b_y(\mathbf{x}))^T$. Let us define the Heaviside function H as

$$H(t) = \int_{-\infty}^{t} \delta(s)ds = \begin{cases} 0 & \text{if } t < 0 \\ \\ 1 & \text{if } t \geq 0 \end{cases}$$

where $\delta(\cdot)$ is the Dirac function. Then, at the time $t = t_{n+1}$, on the edge $\overline{P_{i,j}P_{i+1,j}}$, we can compute

$$H\left(\int_{\overline{P_{i,j}P_{i+1,j}}} \overrightarrow{\mathbf{b}}^{n+1}(\mathbf{x}) \cdot (1,0)^T ds\right) = H\left(\int_{\overline{P_{i,j}P_{i+1,j}}} b_x^{n+1}(\mathbf{x})ds\right)$$

to indicate the horizontal upwind direction. Then we define the x-coordinate of the upwind point ${x_{i+\frac{1}{2},j}^{n+1}}^*$ on the edge $\overline{P_{i,j}P_{i+1,j}}$ for $i = 0, \ldots, N_x - 1$, $j = 0, \ldots, N_y$ and

$n = 0, \ldots, N_t$ as

$$x_{i+\frac{1}{2},j}^{n+1\ *} = H\left(\int_{\overline{P_{i,j}P_{i+1,j}}} b_x^{n+1}(\mathbf{x})ds\right)\left[\alpha_{i+\frac{1}{2},j}^x x_i + (1-\alpha_{i+\frac{1}{2},j}^x)x_{i+1}\right] + \left(1 - H\left(\int_{\overline{P_{i,j}P_{i+1,j}}} b_x^{n+1}(\mathbf{x})ds\right)\right)\left[(1-\alpha_{i+\frac{1}{2},j}^x)x_i + \alpha_{i+\frac{1}{2},j}^x x_{i+1}\right] \quad (3.1)$$

where $\alpha_{i+\frac{1}{2},j}^x$ is a local weight factor. Thus, the upwind point on $\overline{P_{i,j}P_{i+1,j}}$ is the point of coordinates $\left(x_{i+\frac{1}{2},j}^{n+1\ *}, y_j\right)$.

To define the local weight factor, let us indicate with $Pe_{i+\frac{1}{2},j}^x$ the local Peclet's number

$$Pe_{i+\frac{1}{2},j}^x = \max_{x_i \le x \le x_{i+1}} \frac{|b_x(x, y_j, t_{n+1})|}{a(x, y_j, t_{n+1})}\Delta x_{i+1}$$

on $\overline{P_{i,j}P_{i+1,j}}$. Then we set

$$\alpha_{i+\frac{1}{2},j}^x = \begin{cases} \frac{1}{2} & \text{if } Pe_{i+\frac{1}{2},j}^x \le 2 \\ 1 - \frac{1}{Pe_{i+\frac{1}{2},j}^x} & \text{if } Pe_{i+\frac{1}{2},j}^x > 2 \end{cases}$$

In a similar way, we define the y-coordinate $y_{i,j+\frac{1}{2}}^{n+1\ *}$ of the upwind point on the edge $\overline{P_{i,j}P_{i,j+1}}$ as

$$y_{i,j+\frac{1}{2}}^{n+1\ *} = H\left(\int_{\overline{P_{i,j}P_{i,j+1}}} b_y^{n+1}(\mathbf{x})ds\right)\left[\alpha_{i,j+\frac{1}{2}}^y y_j + (1-\alpha_{i,j+\frac{1}{2}}^y)y_{j+1}\right] + \left(1 - H\left(\int_{\overline{P_{i,j}P_{i,j+1}}} b_y^{n+1}(\mathbf{x})ds\right)\right)\left[(1-\alpha_{i,j+\frac{1}{2}}^y)y_j + \alpha_{i,j+\frac{1}{2}}^y y_{j+1}\right] \quad (3.2)$$

where

$$\alpha_{i,j+\frac{1}{2}}^y = \begin{cases} \frac{1}{2} & \text{if } Pe_{i,j+\frac{1}{2}}^y \le 2 \\ 1 - \frac{1}{Pe_{i,j+\frac{1}{2}}^y} & \text{if } Pe_{i,j+\frac{1}{2}}^y > 2 \end{cases}$$

and

$$Pe_{i,j+\frac{1}{2}}^y = \max_{y_j \le y \le y_{j+1}} \frac{|b_y(x_i, y, t_{n+1})|}{a(x_i, y, t_{n+1})}\Delta y_{j+1}$$

Thus, the upwind point on $\overline{P_{i,j}P_{i,j+1}}$ is the point of coordinates $\left(x_i, y_{i,j+\frac{1}{2}}^{n+1\ *}\right)$.

Then, to construct the new control volume, in each cell $\Omega_{i,j}$, we take the midpoint

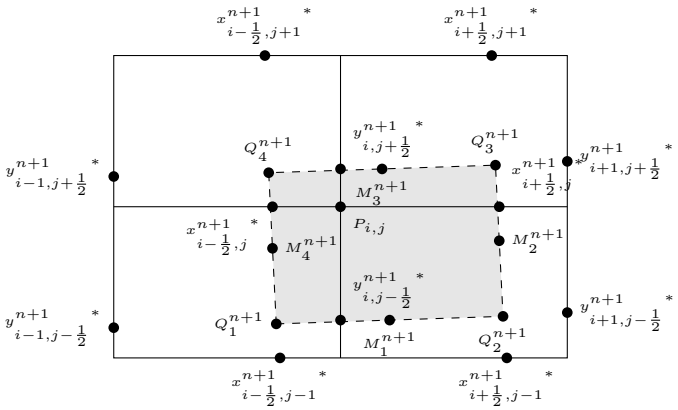

Figure 3.1 Upwind-control volume associated with the interior grid point $P_{i,j}$.

of the upwind points on opposite edges, to obtain the point $Q_{i,j}^{n+1}$ inside the grid cell $\Omega_{i,j}$ as

$$Q_{i,j}^{n+1} = \left(\frac{x_{i-\frac{1}{2},j}^{n+1}{}^* + x_{i-\frac{1}{2},j-1}^{n+1}{}^*}{2}, \frac{y_{i-1,j-\frac{1}{2}}^{n+1}{}^* + y_{i,j-\frac{1}{2}}^{n+1}{}^*}{2} \right)$$

After finding the $Q_{i,j}^{n+1}$'s of the four neighbor grid cells of the grid point $P_{i,j}$, we connect them to form its control volume $\Omega_{i,j}^{n+1*}$ as shown in Figure 3.1. Then the set of the nonstandard control volumes

$$\Omega_{h,n+1}^* = \{\Omega_{i,j}^{n+1*} : i = 1, \ldots, N_x - 1,\, j = 1, \ldots, N_y - 1,\, n = 0, \ldots, N_t - 1\}$$

forms an upwind dual partition of Ω with respect to the rectangulation Ω_h.

3.2 The bilinear discretization scheme

We will find now the bilinear finite volume discretization of the problem (1.1). We choose the trial space U_h to be the space of the piecewise bilinear functions over the rectangular grid Ω_h as in (2.4) and let $\mathbf{P}_\Omega$, $\mathbf{P}$ and $\mathbf{P}_D$ be defined as in (2.1)-(2.3).

Let $\{\phi_{i,j}(\mathbf{x})\}_{P_{i,j}\in\mathbf{P}_\Omega}$ be the set of basis functions of U_h, with

$$\phi_{i,j}(\mathbf{x}) = \begin{cases} 1 & \mathbf{x} = P_{i,j} \\ 0 & \text{otherwise} \end{cases}$$

Then, any $u_h \in U_h$ can be written as

$$u_h(\mathbf{x}, t) = \sum_{P_{i,j}\in\mathbf{P}_\Omega} u_{i,j}\phi_{i,j}(\mathbf{x})$$

where $u_{i,j} = u_h(P_{i,j})$.

Let us set the test function space V_h to be the space of piecewise constant function space over the dual partition $\Omega_h^{n+1^*}$

$$V_h = \{v_h \in \mathrm{L}_2(\bar{\Omega}) : v_h|_{\Omega_{i,j}^{n+1^*}} = \text{constant for any } \Omega_{i,j}^{n+1^*} \in {\Omega_{h,n+1}}^* \text{ and } v_h|_{\Omega_{i,j}^{n+1^*}} = 0 \text{ if } P_{i,j} \in \mathbf{P}_D\}$$

and let $\{\psi_{i,j},\, (i,j) \in \mathbf{P}\}$ be a basis of V_h, where $\psi_{i,j}$ are the characteristic functions of the covolume $\Omega_{i,j}^{n+1^*}$ defined as

$$\psi_{i,j}(\mathbf{x}) = \begin{cases} 1, & \mathbf{x} \in \Omega_{i,j}^{n+1^*} \\ 0, & \mathbf{x} \in \Omega/\Omega_{i,j}^{n+1^*} \end{cases}$$

Multiplying the differential equation of (1.1) by $v_h \in V_h$, integrating over Ω and applying Green's formula on each $\Omega_{i,j}^{n+1^*}$, replacing u with $u_h \in U_h$ and using the Crank-Nicolson scheme, we get the discrete approximation for the problem (1.1): Find $u_h^{n+1} \in U_h$ such that

$$\begin{cases} B_h\left(\frac{u_h^{n+1}-u_h^n}{\Delta t}, v_h\right) + A_h\left(\frac{u_h^{n+1}+u_h^n}{2}, v_h^n\right) = L_h\left(\frac{f^{n+1}+f^n}{2}, v_h\right) \quad \forall v_h \in V_h,\, n = 0, 1, \ldots \\ u_h^0|_{\mathbf{P}_D} = u_0 \end{cases} \tag{3.3}$$

with

$$B_h\left(\frac{u_h^{n+1}-u_h^n}{\Delta t}, v_h\right) = \sum_{P_{i,j}\in\mathbf{P}} v_h(P_{i,j}) \int_{\Omega_{i,j}^{n+1^*}} \left(\frac{u_h^{n+1}-u_h^n}{\Delta t}\right) d\mathbf{x}, \tag{3.4}$$

$$\begin{aligned} A_h\left(\frac{u_h^{n+1}+u_h^n}{2}, v_h^n\right) = & - \sum_{P_{i,j}\in\mathbf{P}} v_h(P_{i,j}) \int_{\partial\Omega_{i,j}^{n+1^*}} \left(\frac{a^{n+1}\nabla u_h^{n+1} + a^n \nabla u_h^n}{2}\right) \cdot \overrightarrow{\nu}_{i,j}^{n+1} ds \\ & + \sum_{P_{i,j}\in\mathbf{P}} v_h(P_{i,j}) \int_{\partial\Omega_{i,j}^{n+1^*}} \frac{(\overrightarrow{\mathbf{b}}^{n+1} \cdot \overrightarrow{\nu}_{i,j}^{n+1})u_h^{n+1} + (\overrightarrow{\mathbf{b}}^{n} \cdot \overrightarrow{\nu}_{i,j}^{n+1})u_h^{n}}{2} ds \\ & + \sum_{P_{i,j}\in\mathbf{P}} v_h(P_{i,j}) \int_{\Omega_{i,j}^{n+1^*}} \frac{r^{n+1}u_h^{n+1} + r^n u_h^n}{2} d\mathbf{x} \end{aligned} \tag{3.5}$$

and

$$L_h\left(\frac{f^{n+1}+f^n}{2}, v_h\right) = \sum_{P_{i,j}\in\mathbf{P}} v_h(P_{i,j}) \int_{\Omega_{i,j}^{n+1^*}} \left(\frac{f^{n+1}+f^n}{2}\right) d\mathbf{x} \tag{3.6}$$

where $\nu_{i,j}^{n+1}$ is the unit outward normal along $\Omega_{i,j}^{n+1^*}$. Setting $v_h = \psi_{i,j}$ in the previous expressions, we obtain

$$\begin{aligned}\int_{\Omega_{i,j}^{n+1^*}} \frac{u_h^{n+1}-u_h^n}{\Delta t} d\mathbf{x} &- \int_{\partial\Omega_{i,j}^{n+1^*}} \frac{(a^{n+1}\nabla u_h^{n+1})\cdot\overrightarrow{\nu}_{i,j}^{n+1} + (a^n\nabla u_h^n)\cdot\overrightarrow{\nu}_{i,j}^{n+1}}{2} ds \\ &+ \int_{\partial\Omega_{i,j}^{n+1^*}} \frac{(\overrightarrow{\mathbf{b}}^{n+1}\cdot\overrightarrow{\nu}_{i,j}^{n+1})u_h^{n+1} + (\overrightarrow{\mathbf{b}}^{n}\cdot\overrightarrow{\nu}_{i,j}^{n+1})u_h^{n}}{2} ds \\ &+ \int_{\Omega_{i,j}^{n+1^*}} \frac{r^{n+1}u_h^{n+1}+r^n u_h^n}{2} d\mathbf{x} = \int_{\Omega_{i,j}^{n+1^*}} \frac{f^{n+1}+f^n}{2} d\mathbf{x}\end{aligned} \tag{3.7}$$

and finally, rearranging the terms, we get

$$\begin{aligned}\int_{\Omega_{i,j}^{n+1^*}} u_h^{n+1} d\mathbf{x} &- \frac{\Delta t}{2}\int_{\partial\Omega_{i,j}^{n+1^*}} (a^{n+1}\nabla u_h^{n+1})\cdot\overrightarrow{\nu}_{i,j}^{n+1} ds \\ &+ \frac{\Delta t}{2}\int_{\partial\Omega_{i,j}^{n+1^*}} (\overrightarrow{\mathbf{b}}^{n+1}\cdot\overrightarrow{\nu}_{i,j}^{n+1})u_h^{n+1} ds + \frac{\Delta t}{2}\int_{\Omega_{i,j}^{n+1^*}} r^{n+1}u_h^{n+1} d\mathbf{x} \\ &= \int_{\Omega_{i,j}^{n+1^*}} u_h^n d\mathbf{x} + \frac{\Delta t}{2}\int_{\partial\Omega_{i,j}^{n+1^*}} (a^n\nabla u_h^n)\cdot\overrightarrow{\nu}_{i,j}^{n+1} ds - \frac{\Delta t}{2}\int_{\partial\Omega_{i,j}^{n+1^*}} (\overrightarrow{\mathbf{b}}^{n}\cdot\overrightarrow{\nu}_{i,j}^{n+1})u_h^n ds \\ &- \frac{\Delta t}{2}\int_{\Omega_{i,j}^{n+1^*}} r^n u_h^n d\mathbf{x} + \frac{\Delta t}{2}\int_{\Omega_{i,j}^{n+1^*}} \frac{f^{n+1}+f^n}{2} d\mathbf{x}\end{aligned} \tag{3.8}$$

To find the approximation of each term of the previous equation, we use second-order accurate midpoint rule. Let us denote with $Q_1^{n+1}Q_2^{n+1}Q_3^{n+1}Q_4^{n+1}$ the covolume associated with the grid point $P_{i,j}$, with M_1^{n+1}, M_2^{n+1}, M_3^{n+1}, M_4^{n+1} the midpoint of $\overline{Q_1^{n+1}Q_2^{n+1}}$, $\overline{Q_2^{n+1}Q_3^{n+1}}$, $\overline{Q_3^{n+1}Q_4^{n+1}}$, $\overline{Q_4^{n+1}Q_1^{n+1}}$ respectively and let M^{n+1} be the center of the quadrilateral $Q_1^{n+1}Q_2^{n+1}Q_3^{n+1}Q_4^{n+1}$, as in Figure 3.1. Then each term of the first member of the previous equation will be approximated as follows:

$$\int_{\Omega_{i,j}^{n+1^*}} u_h^{n+1} d\mathbf{x} \approx u_h^{n+1}(M^{n+1})\ Area(Q_1^{n+1}Q_2^{n+1}Q_3^{n+1}Q_4^{n+1}) \tag{3.9}$$

$$\begin{aligned}-\int_{\partial\Omega_{i,j}^{n+1^*}} (a^{n+1}\nabla u_h^{n+1})\cdot\overrightarrow{\nu}_{i,j}^{n+1} ds \approx &- (\nabla u_h^{n+1}(M_1^{n+1})\cdot\overrightarrow{\nu}^{n+1}_{Q_1^{n+1}Q_2^{n+1}})\int_{\overline{Q_1^{n+1}Q_2^{n+1}}} a^{n+1} ds \\ &- (\nabla u_h^{n+1}(M_2^{n+1})\cdot\overrightarrow{\nu}^{n+1}_{Q_2^{n+1}Q_3^{n+1}})\int_{\overline{Q_2^{n+1}Q_3^{n+1}}} a^{n+1} ds \\ &- (\nabla u_h^{n+1}(M_3^{n+1})\cdot\overrightarrow{\nu}^{n+1}_{Q_3^{n+1}Q_4^{n+1}})\int_{\overline{Q_3^{n+1}Q_4^{n+1}}} a^{n+1} ds \\ &- (\nabla u_h^{n+1}(M_4^{n+1})\cdot\overrightarrow{\nu}^{n+1}_{Q_4^{n+1}Q_1^{n+1}})\int_{\overline{Q_4^{n+1}Q_1^{n+1}}} a^{n+1} ds\end{aligned} \tag{3.10}$$

$$\begin{aligned}\int_{\partial\Omega_{i,j}^{n+1^*}}(\overrightarrow{\mathbf{b}}^{n+1}\cdot\overrightarrow{\nu}_{i,j}^{n+1})u_h^{n+1}ds \approx &+ u_h^{n+1}(M_1^{n+1})\int_{\overline{Q_1^{n+1}Q_2^{n+1}}}\overrightarrow{\mathbf{b}}^{n+1}\cdot\overrightarrow{\nu}_{Q_1^{n+1}Q_2^{n+1}}^{n+1}ds\\ &+ u_h^{n+1}(M_2^{n+1})\int_{\overline{Q_2^{n+1}Q_3^{n+1}}}\overrightarrow{\mathbf{b}}^{n+1}\cdot\overrightarrow{\nu}_{Q_2^{n+1}Q_3^{n+1}}^{n+1}ds\\ &+ u_h^{n+1}(M_3^{n+1})\int_{\overline{Q_3^{n+1}Q_4^{n+1}}}\overrightarrow{\mathbf{b}}^{n+1}\cdot\overrightarrow{\nu}_{Q_3^{n+1}Q_4^{n+1}}^{n+1}ds\\ &+ u_h^{n+1}(M_4^{n+1})\int_{\overline{Q_4^{n+1}Q_1^{n+1}}}\overrightarrow{\mathbf{b}}^{n+1}\cdot\overrightarrow{\nu}_{Q_4^{n+1}Q_1^{n+1}}^{n+1}ds \quad (3.11)\end{aligned}$$

$$\int_{\Omega_{i,j}^{n+1^*}} r^{n+1}u_h^{n+1}d\mathbf{x} \approx u_h^{n+1}(M^{n+1})\int_{Q_1^{n+1}Q_2^{n+1}Q_3^{n+1}Q_4^{n+1}} r^{n+1}d\mathbf{x} \quad (3.12)$$

Similarly, the right hand side becomes

$$\int_{\Omega_{i,j}^{n+1^*}} u_h^n d\mathbf{x} \approx u_h^n(M^{n+1})\ Area(Q_1^{n+1}Q_2^{n+1}Q_3^{n+1}Q_4^{n+1}) \quad (3.13)$$

$$\begin{aligned}\int_{\partial\Omega_{i,j}^{n+1^*}}(a^n\nabla u_h^n)\cdot\overrightarrow{\nu}_{i,j}^{n+1}ds \approx &+ (\nabla u_h^n(M_1^{n+1})\cdot\overrightarrow{\nu}_{Q_1^{n+1}Q_2^{n+1}}^{n+1})\int_{\overline{Q_1^{n+1}Q_2^{n+1}}}a^n ds\\ &+ (\nabla u_h^n(M_2^{n+1})\cdot\overrightarrow{\nu}_{Q_2^{n+1}Q_2^{n+1}}^{n+1})\int_{\overline{Q_2^{n+1}Q_3^{n+1}}}a^n ds\\ &+ (\nabla u_h^n(M_3^{n+1})\cdot\overrightarrow{\nu}_{Q_3^{n+1}Q_4^{n+1}}^{n+1})\int_{\overline{Q_3^{n+1}Q_4^{n+1}}}a^n ds\\ &+ (\nabla u_h^n(M_4^{n+1})\cdot\overrightarrow{\nu}_{Q_4^{n+1}Q_1^{n+1}}^{n+1})\int_{\overline{Q_4^{n+1}Q_1^{n+1}}}a^n ds \quad (3.14)\end{aligned}$$

$$\begin{aligned}-\int_{\partial\Omega_{i,j}^{n+1^*}}(\overrightarrow{\mathbf{b}}^{n}\cdot\overrightarrow{\nu}_{i,j}^{n+1})u_h^{n}ds \approx &- u_h^{n}(M_1^{n+1})\int_{\overline{Q_1^{n+1}Q_2^{n+1}}}\overrightarrow{\mathbf{b}}^{n}\cdot\overrightarrow{\nu}_{Q_1^{n+1}Q_2^{n+1}}^{n+1}ds\\ &- u_h^{n}(M_2^{n+1})\int_{\overline{Q_2^{n+1}Q_3^{n+1}}}\overrightarrow{\mathbf{b}}^{n}\cdot\overrightarrow{\nu}_{Q_2^{n+1}Q_3^{n+1}}^{n+1}ds\\ &- u_h^{n}(M_3^{n+1})\int_{\overline{Q_3^{n+1}Q_4^{n+1}}}\overrightarrow{\mathbf{b}}^{n}\cdot\overrightarrow{\nu}_{Q_3^{n+1}Q_4^{n+1}}^{n+1}ds\\ &- u_h^{n}(M_4^{n+1})\int_{\overline{Q_4^{n+1}Q_1^{n+1}}}\overrightarrow{\mathbf{b}}^{n}\cdot\overrightarrow{\nu}_{Q_4^{n+1}Q_1^{n+1}}^{n+1}ds \quad (3.15)\end{aligned}$$

$$-\int_{\Omega_{i,j}^{n+1^*}} r^{n}u_h^{n}d\mathbf{x} \approx -u_h^{n}(M^{n+1})\int_{Q_1^{n+1}Q_2^{n+1}Q_3^{n+1}Q_4^{n+1}} r^{n}d\mathbf{x} \quad (3.16)$$

We still need to evaluate $u_h^{n+1}(M^{n+1})$, $u_h^n(M^{n+1})$ and $u_h^{n+1}(M_k^{n+1})$, $u_h^n(M_k^{n+1})$, $\frac{\partial u_h^{n+1}}{\partial x}(M_k^{n+1})$, $\frac{\partial u_h^{n+1}}{\partial y}(M_k^{n+1})$, $\frac{\partial u_h^n}{\partial x}(M_k^{n+1})$, $\frac{\partial u_h^n}{\partial y}(M_k^{n+1})$, for $k = 1, 2, 3, 4$. Since $M_k^{n+1} = (\hat{x}, \hat{y})$ must fall in one of the four neighbor cells of $P_{i,j}$, say $P_{\hat{i},\hat{j}}P_{\hat{i}-1,\hat{j}}P_{\hat{i}-1,\hat{j}-1}P_{\hat{i},\hat{j}-1}$, we can use the bilinear interpolation properties to get the following formulas for $k = 1, 2, 3, 4$:

$$u_h^{n+1}(M_k^{n+1}) = (1-\gamma_x)(1-\gamma_y)u_{\hat{i}-1,\hat{j}-1}^{n+1} + \gamma_x\gamma_y u_{\hat{i},\hat{j}}^{n+1} + \gamma_x(1-\gamma_y)u_{\hat{i},\hat{j}-1}^{n+1} + (1-\gamma_x)\gamma_y u_{\hat{i}-1,\hat{j}}^{n+1}$$

$$u_h^n(M_k^{n+1}) = (1-\gamma_x)(1-\gamma_y)u_{\hat{i}-1,\hat{j}-1}^{n} + \gamma_x\gamma_y u_{\hat{i},\hat{j}}^{n} + \gamma_x(1-\gamma_y)u_{\hat{i},\hat{j}-1}^{n} + (1-\gamma_x)\gamma_y u_{\hat{i}-1,\hat{j}}^{n}$$

$$\frac{\partial u_h^{n+1}}{\partial x}(M_k^{n+1}) = \frac{1}{\Delta x_{\hat{i}-1}}\left(\gamma_y u_{\hat{i},\hat{j}}^{n+1} + (1-\gamma_y)u_{\hat{i},\hat{j}-1}^{n+1} - \gamma_y u_{\hat{i}-1,\hat{j}}^{n+1} - (1-\gamma_y)u_{\hat{i}-1,\hat{j}-1}^{n+1}\right)$$

$$\frac{\partial u_h^{n+1}}{\partial y}(M_k^{n+1}) = \frac{1}{\Delta y_{\hat{i}-1}}\left(\gamma_x u_{\hat{i},\hat{j}}^{n+1} + (1-\gamma_x)u_{\hat{i}-1,\hat{j}}^{n+1} - \gamma_x u_{\hat{i},\hat{j}-1}^{n+1} - (1-\gamma_x)u_{\hat{i}-1,\hat{j}-1}^{n+1}\right)$$

$$\frac{\partial u_h^{n}}{\partial x}(M_k^{n+1}) = \frac{1}{\Delta x_{\hat{i}-1}}\left(\gamma_y u_{\hat{i},\hat{j}}^{n} + (1-\gamma_y)u_{\hat{i},\hat{j}-1}^{n} - \gamma_y u_{\hat{i}-1,\hat{j}}^{n} - (1-\gamma_y)u_{\hat{i}-1,\hat{j}-1}^{n}\right)$$

$$\frac{\partial u_h^{n}}{\partial y}(M_k^{n+1}) = \frac{1}{\Delta y_{\hat{i}-1}}\left(\gamma_x u_{\hat{i},\hat{j}}^{n} + (1-\gamma_x)u_{\hat{i}-1,\hat{j}}^{n} - \gamma_x u_{\hat{i},\hat{j}-1}^{n} - (1-\gamma_x)u_{\hat{i}-1,\hat{j}-1}^{n}\right)$$

where

$$\gamma_x = \frac{\hat{x} - x_{\hat{i}-1}}{\Delta x_{\hat{i}-1}}, \qquad \gamma_y = \frac{\hat{y} - y_{\hat{j}-1}}{\Delta y_{\hat{j}-1}}$$

Then we get a discrete system in $u(P_{i,j})$ for $P_{i,j} \in \mathbf{P}$ at the time $t = t_{n+1}$.

As for the steady-state equation (see [27]), this method is second-order accurate and it is stable also for convection-dominated problems. We notice that if the Peclet's numbers of the given parabolic problem are smaller than or equal to 2, then the control volume of the bilinear scheme will reduce to the covolume defined for the central scheme and the bilinear discretization will coincide with the central scheme.

Chapter 4

Numerical results

In this chapter, we present some numerical examples to demonstrate the convergence and stability of the bilinear covolume-upwind finite volume method applied to parabolic partial differential equations. We will compare this method with the central and the upwind schemes, showing that the non-physical oscillations that may arise when solving convection dominated problems with the central scheme, disappear when using the bilinear CUFVM. Moreover, we will show also that the bilinear CUFVM is second-order in the L^2 norm and first-order in the H^1 norm.

Let us define the error e_h^n as

$$e_h^n = u(t_n) - u_h^n$$

for $n = 0, 1, ..$ and the measures associated with the mesh Ω_h

$$\| e_h^n \|_{L^\infty} = \max |e_h^n| \tag{4.1}$$

$$\| e_h^n \|_{L^2} = \left(\sum_{i,j} \int_{\Omega_{i,j}} |e_h^n|^2 d\mathbf{x} \right)^{\frac{1}{2}} \tag{4.2}$$

$$|e_h^n|_{H^1} = \left(\sum_{i,j} \int_{\Omega_{i,j}} |\nabla e_h^n|^2 d\mathbf{x} \right)^{\frac{1}{2}} \tag{4.3}$$

$$|e_h^n|_{1,\Omega_h} = \left(\sum_{i,j} |\nabla e_h^n \left(x_{i-\frac{1}{2}}, y_{j-\frac{1}{2}} \right)|^2 \Delta x_i \Delta y_j \right)^{\frac{1}{2}} \tag{4.4}$$

For the following examples, we choose the time interval $[0, T]$ to be the interval $[0, 1]$ and $\Omega = [0, 1] \times [0, 1]$ and we solve the model problem (1.1) using the central, the upwind and the bilinear covolume-upwind schemes respectively. We computed

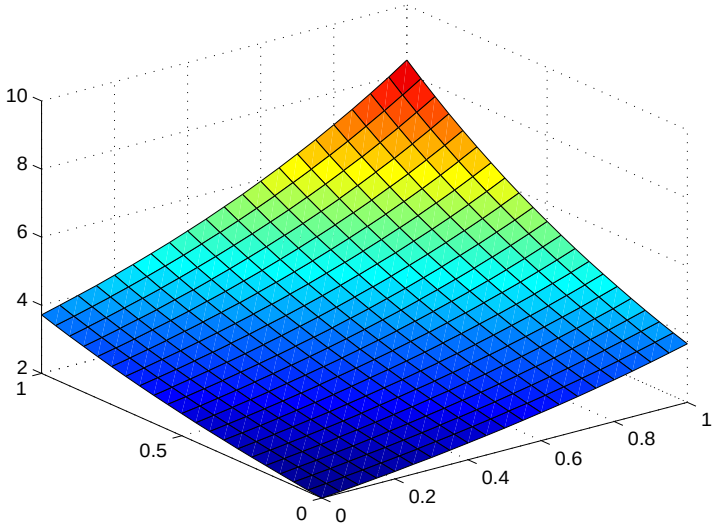

Figure 4.1 Plot of the exact solution of Example 4.1

the errors at the time $t = t_{N_t}$ using the measures defined above and we found also the condition numbers of the discretized system to prove stability of the discretized systems that results from the bilinear CUFVM. For every example, we used time discretization with sizes $N_t = 10, 20, 40, 80$ and uniform spatial grids with sizes $N_x \times N_y = 10 \times 10$, 20×20, 40×40 and 80×80.

Example 4.1. In this example, the exact solution is chosen to be the function

$$u(x, y, t) = 1 + te^{x+y}$$

This is a smooth function and its graph is displayed on Figure 4.1. The convection term is defined as $\overrightarrow{\mathbf{b}} = (2, 1)$ and the reaction coefficient is set equal to $r(x, y, t) = 1$. The diffusion coefficient a is set equal to 1, 10^{-3} and 10^{-8} respectively. Then the condition (1.2) is satisfied since $\nabla \cdot \overrightarrow{\mathbf{b}} = 0$. The source function f is determined by the choice of u and equation (1.1).

The results for this example are shown on Tables 4.1, 4.2 and 4.3 for the CFVM, the UFVM and the bilinear CUFVM respectively. From the tables, we can observe

Table 4.1 Numerical results for Example 4.1 using the CFVM

a	N_t	$N_x \times N_y$	$\| e_h \|_{L^\infty}$	CR	$\| e_h \|_{L^2}$	CR	$\| e_h \|_{H^1}$	CR	$\| e_h \|_{1,\Omega_h}$	CR
1	10	10×10	1.510e-2	–	5.500e-3	–	1.304e-1	–	7.600e-3	–
	20	20×20	3.900e-3	1.95	1.400e-3	1.97	6.520e-2	1.00	1.900e-3	2.00
	40	40×40	1.000e-3	1.96	3.449e-4	2.02	3.260e-2	1.00	4.771e-4	1.99
	80	80×80	2.528e-4	1.98	8.625e-4	2.00	1.630e-2	1.00	1.193e-4	1.99
10^{-3}	10	10×10	1.490e-2	–	5.300e-3	–	1.306e-1	–	9.600e-3	–
	20	20×20	3.900e-3	1.93	1.300e-3	2.03	6.530e-2	1.00	3.112e-3	1.63
	40	40×40	9.826e-4	1.99	3.303e-4	1.98	3.260e-2	1.00	1.100e-3	1.49
	80	80×80	2.483e-4	1.98	8.255e-5	2.00	1.630e-2	1.00	3.213e-4	1.77
10^{-8}	10	10×10	1.490e-2	–	5.320e-3	–	1.306e-1	–	9.901e-3	–
	20	20×20	3.900e-3	1.93	1.301e-3	2.03	6.530e-2	1.00	3.702e-3	1.42
	40	40×40	9.805e-4	1.99	3.316e-4	1.97	3.260e-2	1.00	1.610e-3	1.21
	80	80×80	2.472e-4	1.99	8.287e-5	2.00	1.630e-2	1.00	7.884e-4	1.02

that, for every choice of a, the bilinear CUFVM is second-order in $\| e_h^n \|_{L^\infty}$ and $\| e_h^n \|_{L^2}$, while it is first-order convergent in $|e_h^n|_{H^1}$, as the central scheme. Using the UFVM, instead, we get the same orders of convergence only in the case $a = 1$, while it becomes first-order convergent in $\| e_h^n \|_{L^\infty}$ and $\| e_h^n \|_{L^2}$ and half-order convergent in $|e_h^n|_{H^1}$ for the other two choices of a.

The results show also that the values for $\| e_h^n \|_{L^\infty}$ and $\| e_h^n \|_{L^2}$ obtained with the bilinear CUFVM are slightly smaller than the corresponding values obtained using the central scheme and very small if compared to those found using the UFVM. Moreover, we can notice that the convergence rates for $|e_h^n|_{1,\Omega_h}$ are equal to 2 for the case $a = 1$, which indicates the superconvergence of the bilinear CUFVM, and they became equal to 1.5 for the case $a = 10^{-3}$ and 10^{-8}. The convergence rates for $|e_h^n|_{1,\Omega_h}$ are equal to 2 for $a = 1$ also for the central and the upwind schemes, but they degenerate to 1 and 0.5 respectively for the convection-dominate problems.

Condition numbers of the discrete systems obtained using the bilinear CUFVM are shown in Table 4.3 and their plot is given in Figure 4.2. We notice that they increase by a rate of almost 4.5 for the case $a = 1$, between 2 and 4 for the case $a = 10^{-3}$ and of roughly 8 for the strongly convection-dominated case $a = 10^{-8}$. Moreover, we observe that condition numbers increase as the diffusion coefficient a becomes smaller (see Figure 4.2).

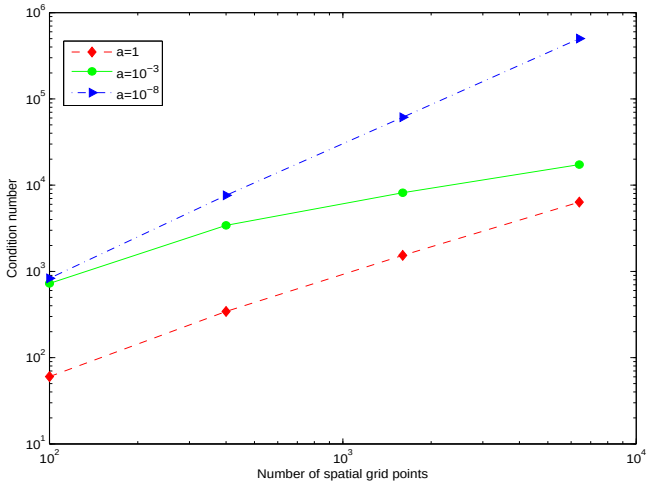

Figure 4.2 Plot of the condition numbers of the discrete systems obtained using the bilinear CUFVM in Example 4.1

Table 4.2 Numerical results for Example 4.1 using the UFVM

a	N_t	$N_x \times N_y$	$\| e_h \|_{L^\infty}$	CR	$\| e_h \|_{L^2}$	CR	$\| e_h \|_{H^1}$	CR	$\| e_h \|_{1,\Omega_h}$	CR
1	10	10×10	1.510e-2	–	5.500e-3	–	1.304e-1	–	7.600e-3	–
	20	20×20	3.900e-3	1.95	1.400e-3	1.97	6.520e-2	1.00	1.900e-3	2.00
	40	40×40	1.000e-3	1.96	3.449e-4	2.02	3.260e-2	1.00	4.771e-4	1.99
	80	80×80	2.528e-4	1.98	8.625e-4	2.00	1.630e-2	1.00	1.193e-4	1.99
10^{-3}	10	10×10	3.549e-1	–	1.231e-1	–	1.025	–	1.004	–
	20	20×20	2.043e-1	0.79	7.150e-2	0.78	7.972e-1	0.36	7.896e-1	0.35
	40	40×40	1.066e-1	0.94	3.741e-2	0.93	5.761e-1	0.47	5.734e-1	0.46
	80	80×80	5.170e-2	1.04	1.810e-2	1.05	3.906e-1	0.56	3.896e-1	0.56
10^{-8}	10	10×10	3.604e-1	–	1.251e-1	–	1.041	–	1.019	–
	20	20×20	2.108e-1	0.77	7.380e-2	0.76	8.224e-1	0.34	8.148e-1	0.32
	40	40×40	1.137e-1	0.89	3.990e-2	0.89	6.142e-1	0.42	6.115e-1	0.41
	80	80×80	5.910e-2	0.94	2.071e-2	0.95	4.463e-1	0.46	4.453e-1	0.46

Example 4.2. In this example, the exact solution is defined as

$$u(x, y, t) = 10e^{-5[(x-0.5)^2+(y-0.5)^2+(t-0.5)^2]}$$

The convection term is set to be equal to $\overrightarrow{\mathbf{b}} = (2 - x^2yt, 1 + xy^2t)$ and the reaction coefficient is again set equal to $r(x, y, t) = 1$. The diffusion coefficient a is again equal to 1, 10^{-3} and 10^{-8} respectively. Then the condition (1.2) is satisfied since also for this example we have $\nabla \cdot \overrightarrow{\mathbf{b}} = 0$. The source function f is determined by the choice of u and equation (1.1).

For this example, the exact solution is plotted in Figure 4.3 and the value of the

Table 4.3 Numerical results for Example 4.1 using bilinear CUFVM

a	N_t	$N_x \times N_y$	$\| e_h \|_{L^\infty}$	CR	$\| e_h \|_{L^2}$	CR	$\| e_h \|_{H^1}$	CR	$\| e_h \|_{1,\Omega_h}$	CR	Cond
1	10	10×10	1.510e-2	–	5.500e-3	–	1.304e-1	–	7.600e-3	–	6.02e+1
	20	20×20	3.900e-3	1.95	1.400e-3	1.97	6.520e-2	1.00	1.900e-3	2.00	3.43e+2
	40	40×40	1.000e-3	1.96	3.449e-4	2.02	3.260e-2	1.00	4.771e-4	1.99	1.53e+3
	80	80×80	2.528e-4	1.98	8.625e-4	2.00	1.630e-2	1.00	1.193e-4	1.99	6.36e+3
10^{-3}	10	10×10	1.440e-2	–	3.801e-3	–	1.318e-1	–	2.090e-2	–	7.25e+2
	20	20×20	3.702e-3	1.96	8.803e-4	2.11	6.560e-2	1.01	7.501e-3	1.48	3.41e+3
	40	40×40	9.493e-4	1.96	2.108e-4	2.06	3.270e-2	1.00	2.701e-3	1.47	8.17e+3
	80	80×80	2.395e-4	1.99	5.183e-5	2.02	1.630e-2	1.00	9.326e-4	1.53	1.73e+4
10^{-8}	10	10×10	1.440e-2	–	3.810e-3	–	1.318e-1	–	2.090e-2	–	8.32e+2
	20	20×20	3.702e-3	1.96	8.793e-4	2.11	6.560e-2	1.01	7.510e-3	1.48	7.62e+3
	40	40×40	9.490e-4	1.96	2.101e-4	2.06	3.270e-2	1.00	2.702e-3	1.47	6.12e+4
	80	80×80	2.393e-4	1.99	5.124e-5	2.03	1.631e-2	1.00	9.503e-4	1.51	5.01e+5

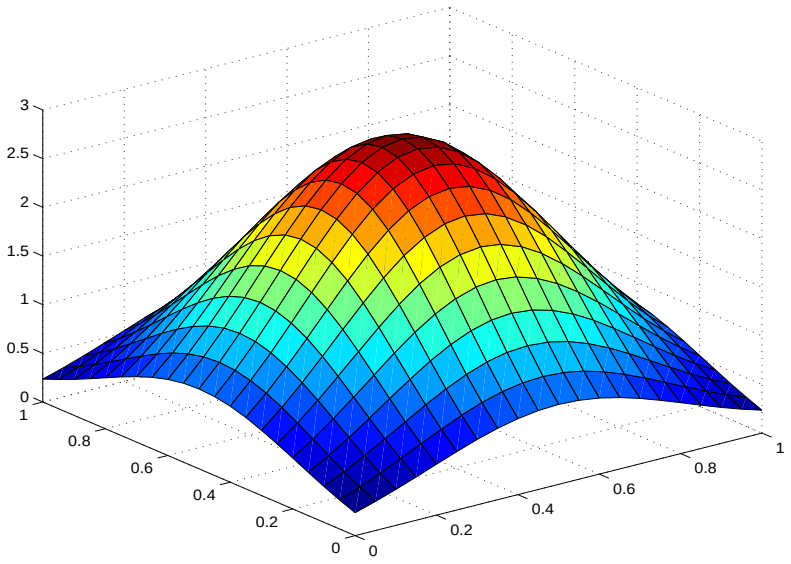

Figure 4.3 Plot of the exact solution of Example 4.2

errors and the convergence rates for the central, upwind and bilinear covolume-upwind schemes are shown in Tables 4.4, 4.5, 4.6 respectively. We notice similar results for the convergence rates to those of the previous example. In this example, we can see that the values of the error for every measure obtained with the bilinear CUFVM are much smaller than the corresponding ones resulting from the application of the central and the upwind schemes. In this example, condition numbers for the discrete systems produced by the bilinear CUFVM are shown in Table 4.6 and their plot can be found in Figure 4.4. Here, condition numbers for all the choices of a are similar or slightly larger than those of Example 4.1.

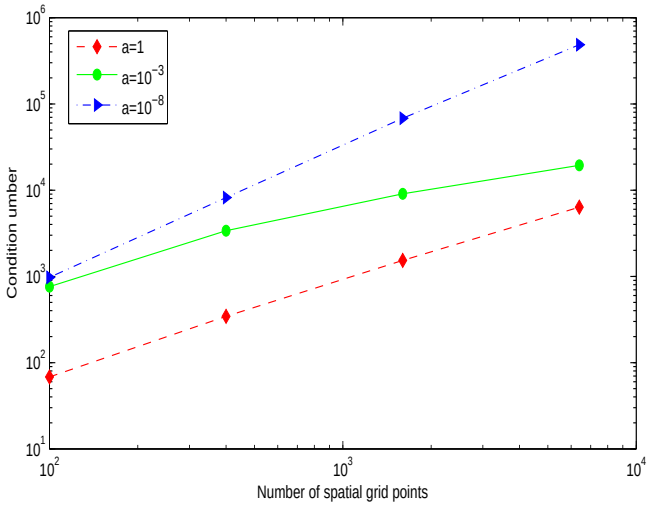

Figure 4.4 Plot of the condition numbers of the discrete systems obtained using the bilinear CUFVM in Example 4.2

Table 4.4 Numerical results for Example 4.2 using the CFVM

a	N_t	$N_x \times N_y$	$\| e_h \|_{L^\infty}$	CR	$\| e_h \|_{L^2}$	CR	$\| e_h \|_{H^1}$	CR	$\| e_h \|_{1,\Omega_h}$	CR
1	10	10×10	3.580e-2	–	9.903e-3	–	4.936e-1	–	3.040e-2	–
	20	20×20	9.210e-2	1.96	2.500e-3	1.98	2.475e-1	0.99	7.602e-3	2.00
	40	40×40	2.303e-3	2.00	6.188e-4	2.01	1.237e-1	0.99	1.901e-3	2.00
	80	80×80	5.743e-4	2.00	1.547e-4	2.00	6.190e-2	0.99	4.790e-4	1.99
10^{-3}	10	10×10	2.778e-1	–	7.740e-2	–	1.355e+0	–	9.788e-1	–
	20	20×20	7.370e-2	1.91	1.810e-2	2.10	4.804e-1	1.49	3.711e-1	1.40
	40	40×40	1.671e-2	2.14	4.401e-3	2.04	1.839e-1	1.38	1.347e-1	1.46
	80	80×80	3.920e-3	2.10	1.101e-3	2.00	7.35e-2	1.32	3.960e-2	1.77
10^{-8}	10	10×10	2.853e-1	–	8.100e-2	–	1.628e+0	–	1.149e+0	–
	20	20×20	8.020e-2	1.83	1.990e-2	2.02	8.036e-1	1.02	5.788e-1	0.99
	40	40×40	2.020e-2	1.99	5.003e-3	1.99	4.000e-1	1.01	2.882e-1	1.01
	80	80×80	5.101e-3	1.98	1.201e-3	2.06	1.997e-1	1.00	1.438e-1	1.00

Example 4.3. In this example, the exact solution is chosen to be the function

$$u(x, y, t) = \frac{t}{1 + e^{-100(\sqrt{x^2+y^2}-0.8)}}$$

The convection and the reaction terms are the same of those of the previous example. Again, the diffusion coefficient a is set equal to 1, 10^{-3} and 10^{-8}. The source function f is determined by the choice of u and equation (1.1).

The exact solution for this example is shown in Figure 4.5. The graph shows that the function is a smooth function, but its values change sharply across the circle

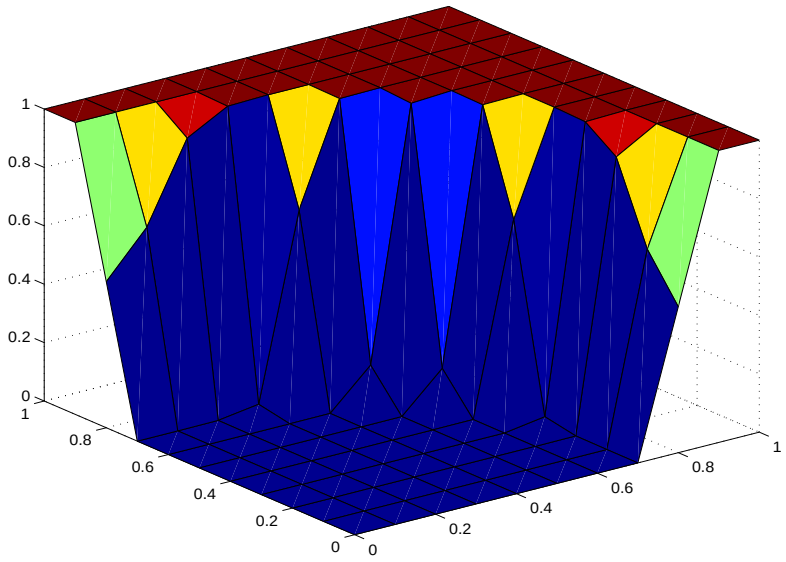

Figure 4.5 Plot of the exact solution of Example 4.3

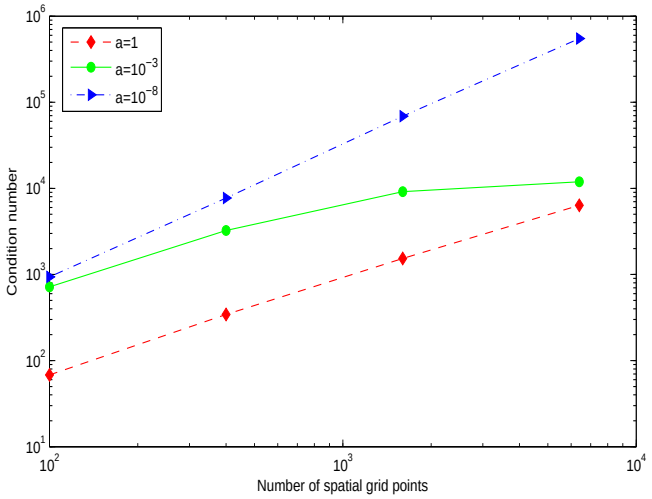

Figure 4.6 Plot of the condition numbers of the discrete systems obtained using the bilinear CUFVM in Example 4.3

Table 4.5 Numerical results for Example 4.2 using the UFVM

a	N_t	$N_x \times N_y$	$\| e_h \|_{L^\infty}$	CR	$\| e_h \|_{L^2}$	CR	$\| e_h \|_{H^1}$	CR	$\| e_h \|_{1,\Omega_h}$	CR
1	10	10×10	3.580e-2	–	9.903e-3	–	4.936e-1	–	3.040e-2	–
	20	20×20	9.210e-2	1.96	2.500e-3	1.98	2.475e-1	0.99	7.602e-3	2.00
	40	40×40	2.303e-3	2.00	6.188e-4	2.01	1.237e-1	0.99	1.901e-3	2.00
	80	80×80	5.743e-4	2.00	1.547e-4	2.00	6.190e-2	0.99	4.790e-4	1.99
10^{-3}	10	10×10	5.421e-1	–	1.314e-1	–	1.545e+0	–	1.427e+0	–
	20	20×20	3.980e-1	0.40	9.700e-2	0.44	1.366e+0	0.18	1.329e+0	0.10
	40	40×40	2.372e-1	0.75	5.810e-2	0.74	1.070e+0	0.35	1.058e+0	0.33
	80	80×80	1.237e-1	0.94	3.041e-2	0.93	7.620e-1	0.49	7.576e-1	0.48
10^{-8}	10	10×10	5.503e-1	–	1.334e-1	–	1.566e+0	–	1.448e+0	–
	20	20×20	4.098e-1	0.42	1.000e-1	0.41	1.406e+0	0.15	1.369e+0	0.06
	40	40×40	2.516e-1	0.70	6.180e-2	0.69	1.135e+0	0.31	1.123e+0	0.28
	80	80×80	1.398e-1	0.85	3.440e-2	0.84	8.617e-1	0.40	8.574e-1	0.39

Table 4.6 Numerical results for Example 4.2 using bilinear CUFVM

a	N_t	$N_x \times N_y$	$\| e_h \|_{L^\infty}$	CR	$\| e_h \|_{L^2}$	CR	$\| e_h \|_{H^1}$	CR	$\| e_h \|_{1,\Omega_h}$	CR	Cond
1	10	10×10	3.580e-2	–	9.903e-3	–	4.936e-1	–	3.040e-2	–	6.81e+1
	20	20×20	9.210e-2	1.96	2.500e-3	1.98	2.475e-1	0.99	7.602e-3	2.00	3.43e+2
	40	40×40	2.303e-3	2.00	6.188e-4	2.01	1.237e-1	0.99	1.901e-3	2.00	1.53e+3
	80	80×80	5.743e-4	2.00	1.547e-4	2.00	6.190e-2	0.99	4.790e-4	1.99	6.36e+3
10^{-3}	10	10×10	6.370e-2	–	1.850e-2	–	5.173e-1	–	1.587e-1	–	7.59e+2
	20	20×20	1.790e-2	1.83	5.100e-3	1.86	2.535e-1	1.03	5.690e-2	1.48	3.38e+3
	40	40×40	4.701e-3	1.93	1.404e-3	1.86	1.253e-1	1.02	2.000e-2	1.51	9.06e+3
	80	80×80	1.200e-3	1.97	3.467e-4	2.01	6.220e-2	1.01	7.100e-3	1.49	1.94e+4
10^{-8}	10	10×10	6.450e-2	–	1.860e-2	–	5.177e-1	–	1.598e-1	–	9.74e+2
	20	20×20	1.800e-2	1.84	5.200e-3	1.84	2.536e-1	1.03	5.730e-2	1.48	8.19e+3
	40	40×40	4.701e-3	1.93	1.404e-3	1.89	1.253e-1	1.02	2.010e-2	1.51	6.83e+4
	80	80×80	1.200e-3	1.97	3.474e-4	2.01	6.230e-2	1.01	7.100e-3	1.50	4.86e+5

$x^2 + y^2 = 0.8^2$. The error measures and the convergence rates for the three methods are reported in Tables 4.7, 4.8, 4.9. We notice that the convergence rates for the three methods are smaller than those of the previous examples, except when the grids become fine enough. We can explain this by the fact that it is difficult to catch the variations of the chosen exact solution function if the mesh sizes are not small enough. The upwind scheme shows more stability than the central scheme, but it is only first-order convergent. Again, the errors given by the bilinear CUFVM are smaller that those of the other two methods and it is still second-order convergent for the convection-dominates problems. Condition numbers for the disctrete systems obtained with the biliear CUFVM for this example are similar to those of the previous Example 4.2 and their plot is shown in Figure 4.6.

Table 4.7 Numerical results for Example 4.3 using the CFVM

a	N_t	$N_x \times N_y$	$\| e_h \|_{L^\infty}$	CR	$\| e_h \|_{L^2}$	CR	$\| e_h \|_{H^1}$	CR	$\| e_h \|_{1,\Omega_h}$	CR
1	10	10×10	4.107e-1	–	9.890e-2	–	3.424e+0	–	2.824e+0	–
	20	20×20	2.365e-1	0.79	5.240e-2	0.92	2.320e+0	0.56	1.351e+0	1.06
	40	40×40	1.477e-1	0.68	4.210e-2	0.32	1.283e+0	0.85	5.488e-1	1.30
	80	80×80	1.104e-1	0.42	4.140e-2	0.02	6.752e-1	0.92	2.585e-1	1.09
10^{-3}	10	10×10	8.285e-1	–	1.906e-1	–	6.615e-1	–	5.258e+0	–
	20	20×20	5.350e-1	0.63	9.030e-2	1.08	6.058e+0	0.13	5.129e+0	0.03
	40	40×40	1.693e-1	1.66	1.520e-2	2.57	2.231e+0	1.44	1.676e+0	1.61
	80	80×80	2.530e-2	2.74	2.001e-3	2.93	6.726e-1	1.73	1.821e-1	3.20
10^{-8}	10	10×10	8.563e-1	–	2.117e-1	–	7.128e+0	–	5.699e+0	–
	20	20×20	7.005e-1	0.29	1.230e-1	0.78	7.675e+0	-0.11	6.659e+0	-0.22
	40	40×40	1.791e-1	1.97	2.880e-2	2.09	3.611e+0	1.09	3.149e+0	1.08
	80	80×80	3.200e-2	2.48	2.801e-3	3.36	7.488e-1	2.27	3.663e-1	3.10

Table 4.8 Numerical results for Example 4.3 using the UFVM

a	N_t	$N_x \times N_y$	$\| e_h \|_{L^\infty}$	CR	$\| e_h \|_{L^2}$	CR	$\| e_h \|_{H^1}$	CR	$\| e_h \|_{1,\Omega_h}$	CR
1	10	10×10	4.107e-1	–	9.890e-2	–	3.424e+0	–	2.824e+0	–
	20	20×20	2.365e-1	0.79	5.240e-2	0.92	2.320e+0	0.56	1.351e+0	1.06
	40	40×40	1.477e-1	0.68	4.210e-2	0.32	1.283e+0	0.85	5.488e-1	1.30
	80	80×80	1.104e-1	0.42	4.140e-2	0.02	6.752e-1	0.92	2.585e-1	1.09
10^{-3}	10	10×10	5.501e-1	–	1.058e-1	–	3.633e+0	–	3.237e+0	–
	20	20×20	3.740e-1	0.56	5.880e-2	0.85	2.748e+0	0.40	2.123e+0	0.61
	40	40×40	2.073e-1	0.85	2.850e-2	1.04	1.652e+0	0.73	1.252e+0	0.76
	80	80×80	9.980e-2	1.05	1.330e-2	1.09	8.555e-1	0.95	6.014e-1	1.06
10^{-8}	10	10×10	5.532e-1	–	1.063e-1	–	3.640e+0	–	3.245e+0	–
	20	20×20	3.831e-1	0.53	5.990e-2	0.86	2.771e+0	0.39	2.151e+0	0.59
	40	40×40	2.164e-1	0.82	2.990e-2	1.00	1.693e+0	0.71	1.307e+0	0.72
	80	80×80	1.110e-1	0.96	1.490e-2	1.00	9.070e-1	0.90	6.733e-1	0.96

Table 4.9 Numerical results for Example 4.3 using bilinear CUFVM

a	N_t	$N_x \times N_y$	$\| e_h \|_{L^\infty}$	CR	$\| e_h \|_{L^2}$	CR	$\| e_h \|_{H^1}$	CR	$\| e_h \|_{1,\Omega_h}$	CR	Cond
1	10	10×10	4.107e-1	–	9.890e-2	–	3.424e+0	–	2.824e+0	–	6.81e+1
	20	20×20	2.365e-1	0.79	5.240e-2	0.92	2.320e+0	0.56	1.351e+0	1.06	3.43e+2
	40	40×40	1.477e-1	0.68	4.210e-2	0.32	1.283e+0	0.85	5.488e-1	1.30	1.53e+3
	80	80×80	1.104e-1	0.42	4.140e-2	0.02	6.752e-1	0.92	2.585e-1	1.09	6.36e+3
10^{-3}	10	10×10	4.737e-1	–	1.143e-1	–	4.601e+0	–	2.990e+0	–	7.17e+2
	20	20×20	2.066e-1	1.19	4.190e-2	1.45	3.036e+0	0.56	1.698e+0	0.82	3.25e+3
	40	40×40	5.950e-2	1.79	8.601e-3	2.28	1.306e+0	1.22	4.211e-1	2.01	9.17e+3
	80	80×80	1.550e-2	1.94	2.100e-3	2.03	6.332e-1	1.04	1.024e-1	2.04	1.19e+4
10^{-8}	10	10×10	5.188e-1	–	1.192e-1	–	4.774e+0	–	3.066e+0	–	9.39e+2
	20	20×20	2.223e-1	1.22	4.710e-2	1.34	3.428e+0	0.48	1.948e+0	0.65	7.74e+3
	40	40×40	5.940e-2	1.90	9.702e-3	2.26	1.517e+0	1.18	5.298e-1	1.88	6.89e+4
	80	80×80	1.540e-2	1.95	2.100e-3	2.21	6.333e-1	1.26	1.024e-1	2.37	5.49e+5

Chapter 5

Conclusions

We studied the bilinear covolume upwind finite volume method for the solution of linear parabolic partial differential equations with pure Dirichelet boundary conditions. We also compared this method with the central and the upwind finite volume methods, using numerical examples and we numerically showed the stability and better convergence of the bilinear CUFVM. However, the rigorous analysis of the stability and the error estimate of the bilinear CUFVM has to be investigated.

Bibliography

[1] N. Afanasyeva, P. Vabishchevich, and M. Vasil'eva, *Unconditionally stable schemes for non-stationary convection-diffusion equations*, CoRR (2012).

[2] G. Akrivis, C. Makridakis, and R. H. Nochetto, *A posteriori error estimates for the crank-nicholson method for the parabolic equations*, Mathematics of Computation **75** (2005), no. 254, 511–531.

[3] Z. Chen, *Finite element methods and their applications*, Springer-Verlag, 2005.

[4] R. Dautray and J. Lion, *Mathematical analysis and numerical methods for science and technology, vol. 6*, Springer-Verlag, 1993.

[5] R. E. Ewing and H. Wang, *A summary of numerical methods for time-dependent advection-dominated partial differential equations*, Journal of Computational and Applied Mathematics **128** (2001), 423–445.

[6] C. Grossmann, H. G. Roos, and M. Stynes, *Numerical treatment of partial differential equations*, Springer-Verlag, 2007.

[7] V. John and E. Schmeyer, *Finite element methods for time-dependent convection-diffusion-reaction equations with small diffusion*, Comput. Methods Appl. Mech. Engrg. **198** (2008), 475–494.

[8] M. K. Kadalbajoo and A. Awasthi, *Crank-nicolson finite difference method based on a midpoint upwind scheme on a non-uniform mesh for time-dependent singularly perturbed convection-diffusion equations*, International Journal of Computer Mathematics **85** (2008), no. 5, 771–790.

[9] P. Knabner and L. Angermann, *Numerical methods for elliptic and parabolic partial differential equations*, Texts in Applied Mathematics, Springer, New York, 2003.

[10] P. Knobloch, *Numerical solution of convection-diffusion equations using a nonlinear method of upwind type*, Journal of Scientific Computing **43** (2008), no. 3, 454–470.

[11] R.D. Lazarov, I.D. Mishev, and P.S. Vassilevski, *Finite volume methods for convection-diffusion problems*, SIAM J. Numer. Anal. **33** (1996), 31–55.

[12] R. Li, Z. Chen, and W. Wu, *Generalized difference methods for differential equations*, Marcel Dekler Inc., 2002.

[13] R. Li and X. Hua, *Generalized upwind difference methods for convection-dominated diffusion problems*, Proceedings of the Second Conference on Numerical Methods for partial differential equations (1991), 83–90.

[14] D. Liang and W. Zhao, *An optimal weighted upwinding covolume method on non-standard grids for convection-diffusion problems in 2d*, International Journal for Numerical Methods in Engineering **67** (2006), 553–577.

[15] G. J. Machado, S. Clain, and R. M. S. Pereira, *Very high-order finite volume method for one-dimensional convection diffusion problems*, Mathematical Models for Engineering Science Ű MMES11 (2011), 207–211.

[16] K. W. Morton, *Numerical solution of convection-diffusion problems*, Chapman and Hall, 1996.

[17] K. W. Morton and I. J. Sobey, *Discretization of a convection-diffusion equation*, IMA Journal of Numerical Analysis **13** (1993), 141–160.

[18] S. V. Patankar, *Numerical heat transfer and fluid flow*, McGraw Hill, 1980.

[19] M. Picasso and V. Prachittham, *An adaptive algorithm for the crank-nicolson scheme applied to a time-dependent convection-diffusion problem*, Journal Of Computational And Applied Mathematics **233** (2009), 1139–1154.

[20] A. A. Samarskii, *On monotone difference schemes for elliptic partial differential equations.*, Zh. Vychisl. Mat. i Mat. Fiz. **5** (1965), 548–551.

[21] A. Shukla, A. K. Singh, and P. Singh, *A recent development of numerical methods for solving convection-diffusion problems*, Applied Mathematics **1** (2011), 1–12.

[22] P. Sun, L.Chen, and J. Xu, *Numerical studies of adaptive finite elements methods for two dimensional convection-dominated problems*, Journal of Scientific Computing **43** (2009), no. 1, 24–43.

[23] T. E. Tezduyar, Y. J. Park, and H. A. Deans, *Finite element procedures for time-dependent convection-diffusion-reaction systems*, International Journal for Numerical Methods in Fluids **7** (1987), 1013–1033.

[24] P. Theeraek, S. Phongthanapanich, and P. Dechaumphai, *Solving convection-diffusion-reaction equation by adaptive finite volume element method*, Mathematics and Computers in Simulation **82** (2011), 220–233.

[25] M. Thongmoon and R. McKibbin, *A comparison of some numerical methods for the advection-diffusion equation*, Res. Lett. Inf. Math. Sci. **10** (2006), 49–62.

[26] R. Verfurth, *Robust a posteriori error estimates for nonstationary convection-diffusion equations*, SIAM Journal of Numerical Analysis **43** (2005), no. 4, 1783–1802.

[27] Xiao Xiao, *Covolume-upwind finite volume approximations for linear elliptic partial differential equations*, Ph.D. thesis, University of South Carolina, 2012.